Generation of Fock states in a superconducting quantum circuit

Max Hofheinz, E. M. Weig,* M. Ansmann, Radoslaw C. Bialczak, Erik Lucero,
M. Neeley, A. D. O'Connell, H. Wang, John M. Martinis, and A. N. Cleland
Department of Physics, University of California, Santa Barbara, CA 93106, USA

Spin systems and harmonic oscillators comprise two archetypes in quantum mechanics[1]. The spin-1/2 system, with two quantum energy levels, is essentially the most nonlinear system found in nature, while the harmonic oscillator represents the most linear, with an infinite number of evenly-spaced quantum levels. A significant difference between these systems is that a two-level spin can be prepared in an arbitrary quantum state using classical excitations, whereas classical excitations applied to an oscillator generate a coherent state, nearly indistinguishable from a classical state[2]. Quantum behaviour in an oscillator is most obvious in Fock states, states with specific numbers of energy quanta, but such states are hard to create[3–7]. Here we demonstrate the first controlled generation of multi-photon Fock states in a solid-state system. We use a superconducting phase qubit[8], a close approximation to a two-level spin system, coupled to a microwave resonator, acting as a harmonic oscillator, to prepare and analyse pure Fock states with up to 6 photons. We contrast the Fock states with coherent states generated using classical pulses applied directly to the resonator.

The difficulty of generating quantum number states in a linear resonator has been overcome by interposing a nonlinear quantum system, such as an ion, between a classical radiation source and the resonator. A classical pulse applied to the nonlinear system creates a quantum state that can subsequently be transferred to the resonator. Repeating this process multiple times results in a quantum number state in the resonator. Such a method was used to deterministically generate Fock number states for the mechanical motion of ions in a harmonic ion trap[3]. The analogous deterministic creation of Fock states in electrodynamic resonators has only been demonstrated for states with one or two photons[5,6], although Fock states with larger photon numbers have been recorded using projective measurements[7,9]. The deterministic creation of pure Fock states in a solid-state system, as described here, represents a significant step forward. Solid-state systems permit highly complex, integrated circuitry to employ such bosonic states in, for example, quantum computational architectures. The integration of microwave resonators with solid state qubits has recently attracted significant interest[10–16], but to date such implementations have only used zero or one photons in the resonator, a regime where the bosonic nature of the linear resonator is not apparent.

The method we use here to generate multi-photon Fock states is scalable to arbitrary photon numbers[3,17], limited only by decoherence times and the speed at which photons can be transferred into the resonator. We generate the Fock states using the qubit as an intermediary between a classical microwave source and the resonator, and following generation, measure the resulting states using the qubit. The Fock states are compared to coherent states, generated by driving the resonator directly with a classical radiation pulse. The complexity of the pulse sequences used to create and analyse the resonator states, and the high fidelity of the resulting measurements, demonstrate a significant advance in the control of superconducting quantum circuits.

Our experimental system (see Fig. 1a) is based on the superconducting phase qubit, a device developed for quantum computation[8]. To a good approximation this qubit is represented by a two-level spin system, with ground state $|\mathrm{g}\rangle$ and excited state $|\mathrm{e}\rangle$. These states are separated in energy by a transition frequency ν_q that may be tuned from about 6 to 9 GHz using an external flux bias. With the application of classical microwave pulses, the quantum state of the qubit can be fully controlled[18]. The qubit state is measured by a destructive single-shot measurement, achieved by applying a flux-bias pulse to the qubit. This pulse causes the $|\mathrm{e}\rangle$ state to tunnel to a state that can be easily distinguished from the $|\mathrm{g}\rangle$ state with a flux measurement performed using a readout dc SQUID[19]. Decoherence of the qubit is characterised by measurement of the energy relaxation time $T_1^\mathrm{q} \approx 550\,\mathrm{ns}$ and phase coherence time $T_2^\mathrm{q} \approx 100\,\mathrm{ns}$.

The qubit is coupled to a superconducting coplanar waveguide resonator, which serves as a harmonic oscillator, with a resonance frequency $\nu_\mathrm{r} = 6.565\,\mathrm{GHz}$. The coupling is achieved using a capacitor, which sets the coupling strength $\Omega/2\pi = 36\,\mathrm{MHz}$, measured using spectroscopy[20] (see Fig. 1b). Achieving strong coupling ($\Omega \gg 1/T_1$) between a phase qubit and a resonator is straightforward[21,22], as the qubit characteristic impedance of $\sim 30\,\mathrm{ohm}$ is well-matched to the resonator characteristic impedance of $\sim 50\,\mathrm{ohm}$. The coupling between the qubit and the resonator can be effectively turned off by biasing the qubit well out of resonance, at a frequency $\nu_\mathrm{q} = \nu_\mathrm{off} = 6.314\,\mathrm{GHz}$ where the coupling is effectively reduced by a factor of $(\nu_\mathrm{r}-\nu_\mathrm{off})^2/(\Omega/2\pi)^2 \approx 50$. Microwaves can also be injected directly into the resonator through a separate microwave feedline. The decoherence times of the resonator were measured to be $T_1^\mathrm{r} \approx 1\,\mu\mathrm{s}$ and $T_2^\mathrm{r} \approx 2\,\mu\mathrm{s} \approx 2T_1^\mathrm{r}$ (to be published). All measurements were performed in a dilution refrigerator operating at $25\,\mathrm{mK} \ll h\nu_{\mathrm{r,q}}/k_\mathrm{B}$ (k_B and h are the Boltzmann and Planck constants, respectively), so thermal noise in this system is negligible.

When the qubit and resonator are tuned off-resonance, so that $|\nu_\mathrm{r} - \nu_\mathrm{q}| \gg \Omega/2\pi$, no photons are exchanged

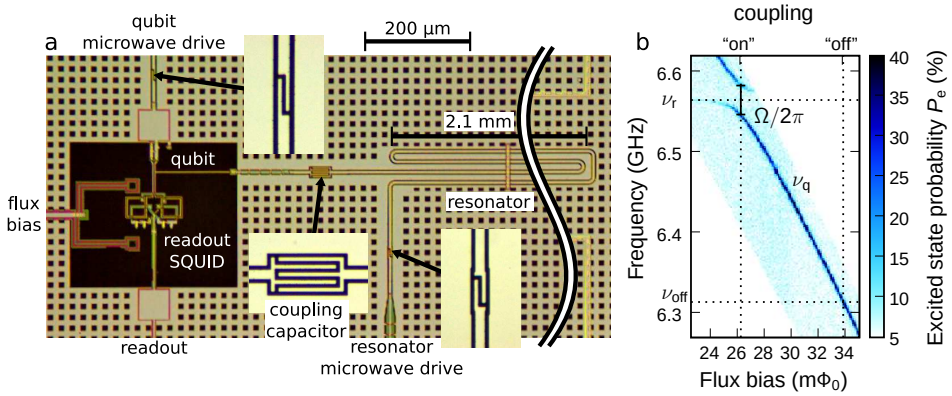

FIG. 1: Device description and spectroscopy. **a,** Photomicrograph of a phase qubit (left) coupled to a coplanar waveguide resonator (right). The resonator has a total length of 8.76 mm. A microwave line capacitively coupled to the qubit is used to inject individual photons into the qubit. A second capacitor between the qubit and resonator couples these two quantum systems, with the resonant interaction controlled by tuning the qubit via a flux bias. The resonator can also be directly excited using a second capacitively-coupled microwave line. **b,** Spectroscopy of qubit and resonator. The false colour image shows the excited state probability P_e of the qubit as a function of driving frequency and flux bias in units of the flux quantum $\Phi_0 = h/2e$. A dark line is seen when the frequency of the microwave drive matches an eigenfrequency of the qubit–resonator system. An avoided crossing appears when the qubit is tuned through the resonator frequency ν_r, shown by the dashed horizontal line. The magnitude of the splitting gives the coupling strength $\Omega/2\pi = 36\,\mathrm{MHz}$. The dashed vertical lines display the qubit operating points for qubit–resonator coupling "on" and "off".

between the qubit and resonator. On resonance, for $\nu_r - \nu_q \ll \Omega/2\pi$, energy can be exchanged between the two systems, and the state of the system can oscillate. The dynamics of energy exchange between the resonator and qubit can be approximated within the rotating-wave approximation by the Jaynes-Cummings model Hamiltonian[23],

$$H_{\mathrm{int}} = \frac{\hbar\Omega}{2}\left(a\sigma_+ + a^\dagger\sigma_-\right), \qquad (1)$$

where $a^\dagger$ and a are the photon creation and annihilation operators for the resonator, and σ_+ and σ_- the qubit raising and lowering operators. If the system is prepared in the state $|\mathrm{g}\rangle|n\rangle$ (qubit in ground state, n photons in the resonator), the system will oscillate between this state and the state $|\mathrm{e}\rangle|n-1\rangle$ at an angular frequency $\Omega_n = \sqrt{n}\Omega$. This $\sqrt{n}$ dependence of the oscillation frequency is the cavity quantum electrodynamic (cQED) equivalent of stimulated emission: A photon is transferred between resonator and qubit more rapidly when more photons are present in the resonator. This increase in oscillation frequency is the key to our measurement of the resonator state.

In order to prepare the resonator in a Fock number state, we begin with the qubit detuned from the resonator and wait a time much larger than $T_1^{\mathrm{r,q}}$, allowing both qubit and resonator to relax to their ground states $|\mathrm{g}\rangle$ and $|0\rangle$. As shown in Fig. 2b, we then apply a Gaussian microwave pulse to the qubit at $\nu_q = \nu_{\mathrm{off}}$ whose amplitude and duration are calibrated to yield the $|\mathrm{e}\rangle$ state. We obtain $\sim 98\,\%$ fidelity for this operation when implemented with properly shaped pulses[24]. The qubit and resonator are then tuned into resonance for a time $\pi/\Omega_1 = \pi/\Omega$ so that the excitation in the qubit is swapped into the resonator. The time and amplitude of the tuning pulse is adjusted to yield the best state transfer, determined by maximising the probability to find the qubit in the $|\mathrm{g}\rangle$ state directly after the pulse. A second microwave pulse is then applied to the qubit to re-prepare it in the $|\mathrm{e}\rangle$ state. The qubit and resonator are brought back into resonance, but for a reduced time $\pi/\Omega_2 = \pi/\sqrt{2}\Omega$. After this procedure is repeated n times, with an appropriate reduction in the transfer time for each successive photon, we obtain a final state $|\mathrm{g}\rangle|n\rangle$ that corresponds to an n-photon Fock state in the resonator.

To analyse the resonator state, we tune the qubit and resonator into resonance for an adjustable interaction time τ and then read out the qubit state. The probability $P_e(\tau)$ for measuring the state $|\mathrm{e}\rangle$ is obtained by averaging 3,000 pulse sequences for each interaction time τ.

The probability is expected to oscillate in the absence of decoherence according to[2]

$$P_e(\tau) = \sum_{n=1}^{\infty} P_n \frac{1-\cos(\Omega_n\tau)}{2}\,, \qquad (2)$$

where P_n is the probability to initially have n photons in the resonator. For a pure Fock state $|n\rangle$, P_e oscillates at the frequency $\Omega_n/2\pi$. When several different $|n\rangle$ states are occupied, the time dependence of $P_e(\tau)$ becomes more complex due to the irrational ratios of the oscillation frequencies Ω_n. Note that although P_0 does not enter Eq. (2) directly, it is given by the time average $\overline{P_e} = \sum_{n=1}^{\infty} P_n/2 = (1-P_0)/2$.

The experimental time dependence of $P_e(\tau)$ is dis-

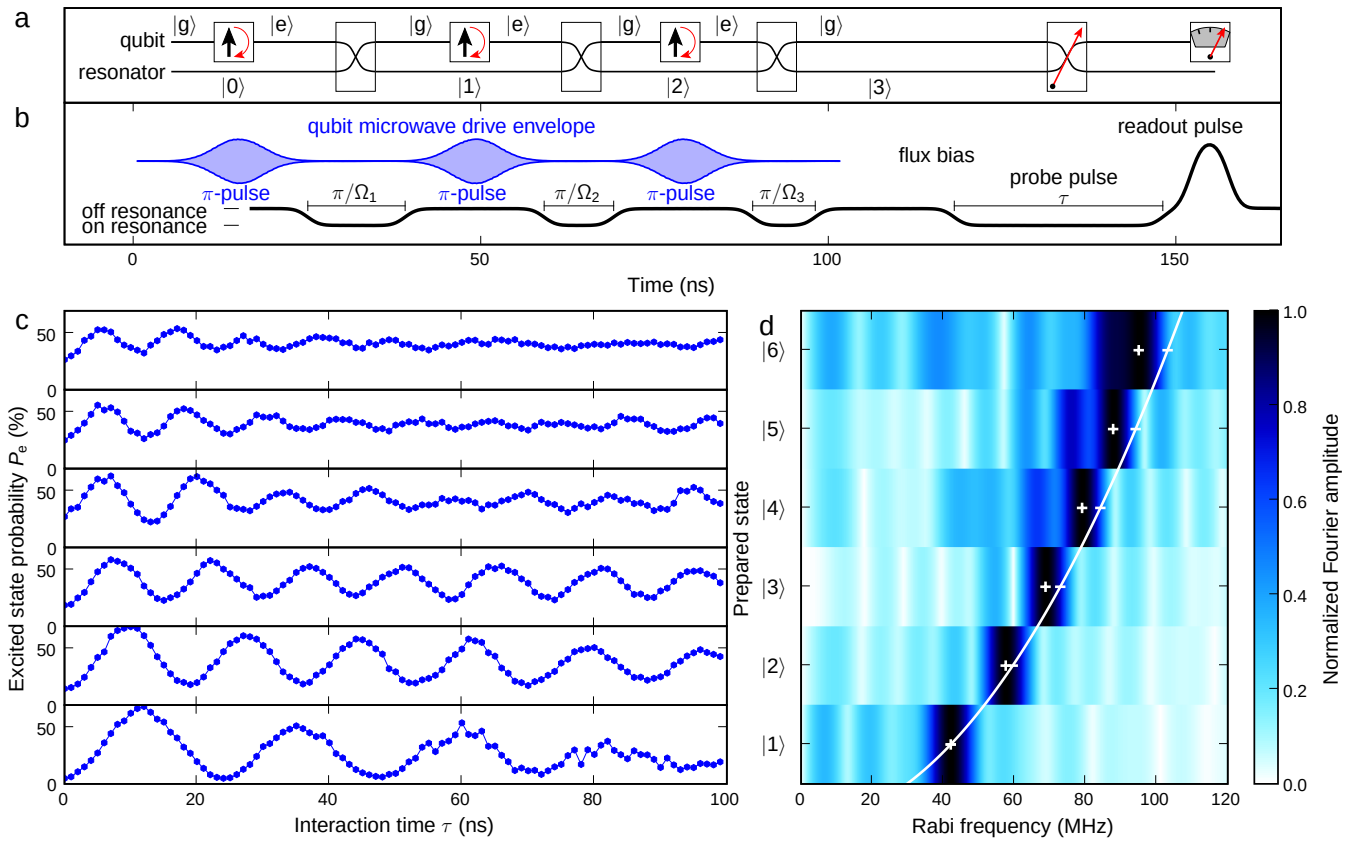

FIG. 2: Preparation and measurement of Fock states. **a,** Quantum program and **b,** pulse sequence for the qubit microwave signal and flux bias used to implement it. An excitation is created in the qubit with a resonant microwave pulse and then transferred into the resonator by tuning the qubit into resonance for half an oscillation period. This sequence is repeated until the desired photon number is reached, 3 in the example depicted here. The length of the tuning pulse decreases as $1/\sqrt{n}$ with the number of photons n. To analyse the resonator state the qubit is tuned into resonance for a variable interaction time τ and the qubit state is finally read out but applying a high flux bias pulse that makes the excited state tunnel into a state which can be easily distinguished from the ground state. **c,** Plot of the probability of the excited qubit state P_e versus interaction time τ for Fock states from $n = 1$ to 6. The time traces show sinusoidal oscillations with a period that shortens with increasing photon number n. **d,** The false colour image shows the Fourier amplitude of the traces in panel c, showing a clear peak at the n-photon oscillation frequency Ω_n, indicating the high purity of the Fock states. The white line indicates the $\sqrt{n}$ scaling of the oscillation frequency expected from the Jaynes-Cummings model in Eq. (1). The Fourier transform was taken with a 100 ns rectangular window, after subtracting the trace average.

played in Fig. 2c for Fock states from $n = 1$ to 6. The time traces are approximately sinusoidal, indicating from Eq. (2) that for each initial state, one photon number dominates in the resonator state. The oscillations have large amplitude up to $n = 3$. Both the amplitude and the decay time decrease with increasing photon number n because the lifetime of an n-photon Fock state decreases as T_1^r/n^{25} and the time needed to create such a state increases as n. At $n = 6$, the lifetime of the Fock state and the length of the preparation sequence are comparable.

The period of the oscillations clearly decreases with n. The period of the $|4\rangle$ state, for example, is approximately half the period of the $|1\rangle$ state, as expected from the $\sqrt{n}$ scaling of the oscillation frequency. A more quantitative analysis of this dependence is shown in Fig. 2d, where the Fourier transforms of the time traces are plotted: Each displays a clear peak at a single frequency, which scales approximately as $\sqrt{n}$. The actual frequency dependence is slightly slower, an effect we attribute to higher energy qubit states not included in the approximate Hamiltonian in Eq. (1). We note that a similar deviation has been observed in the coupling between the internal and translational degrees of freedom of harmonically-trapped ions[3].

We next highlight the non-classical features of the Fock states by comparing them to coherent states, the quan-

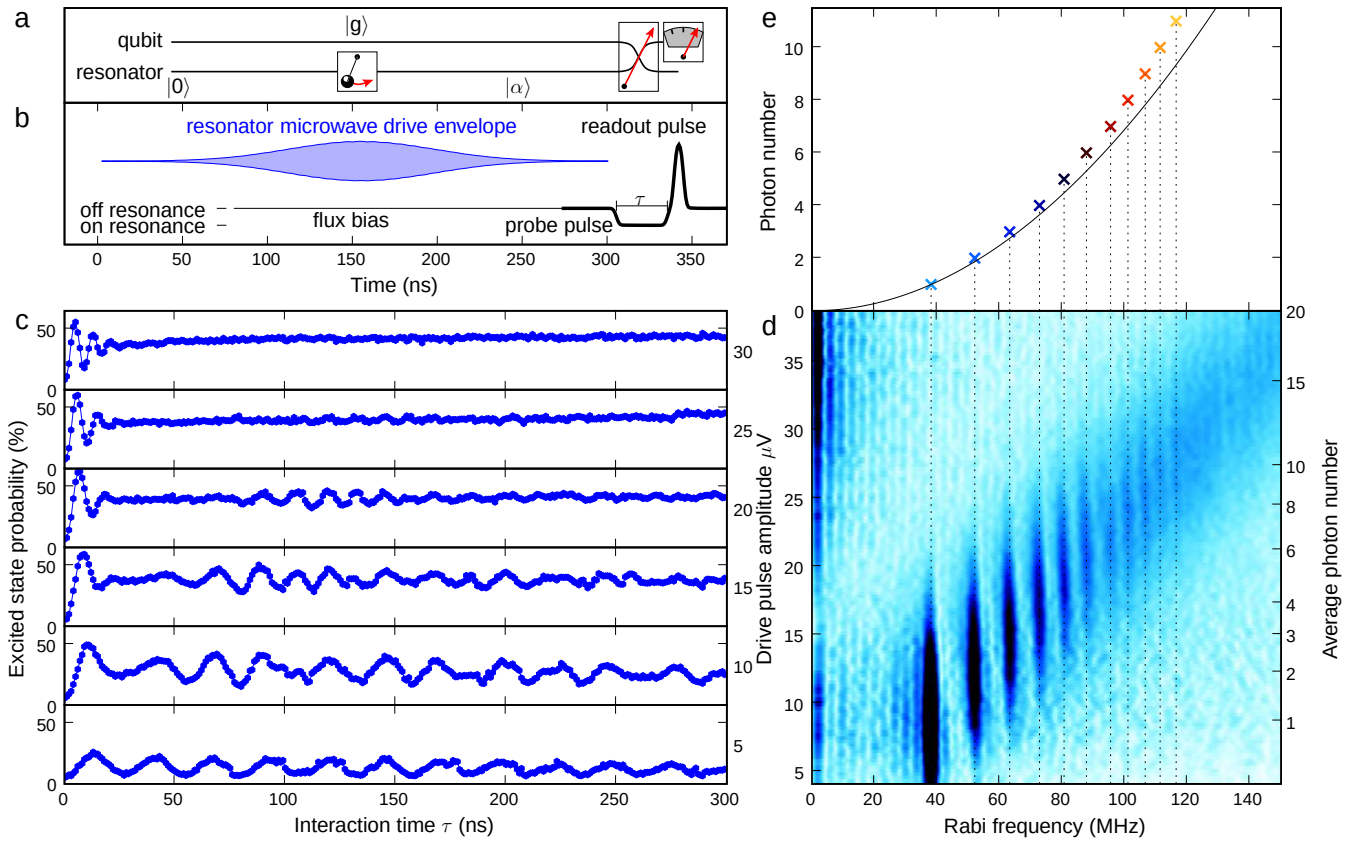

FIG. 3: Preparation and measurement of coherent states. **a,** Quantum program and **b,** pulse sequence of the resonator microwave drive and the qubit bias used to implement it. A 100 ns FWHM Gaussian pulse with varying amplitude is directly applied to the resonator and creates a coherent state. The qubit, in its ground state, is then brought into resonance for a variable interaction time τ and measured, exactly as for the Fock state measurement. **c,** Plot of the excited-state probability P_e versus interaction time τ for six different microwave amplitudes. The time traces are aperiodic because of the irrational ratios in the oscillation times for the different photon number states $|n\rangle$ comprising the coherent state. **d,** Fourier transform of the data in panel c, obtained with a 300 ns rectangular window function, after subtracting the averaged value. Dark colour indicates high amplitude. The data have been smoothed in the drive-pulse direction with a $\sigma = 0.2\,\mu$V Gaussian low-pass filter. The Fourier spectrum reveals a sharp peak at each number-state frequency from $n = 1$ to 11. **e,** Evolution of the frequency of Fourier peaks with photon number n, compared to the expected $\sqrt{n}$ scaling. Deviations from theory are consistent with the Fock-state data in Fig. 2d.

tum equivalent of classical oscillations that are created when a harmonic oscillator is driven directly with a classical signal. To create such states we drive the resonator with a Gaussian-shaped resonant microwave pulse with a full-width at half maximum envelope (FWHM) of 100 ns (see Fig. 3b) and a range of amplitudes. The qubit is not involved in this state preparation and stays in the ground state. The readout of the resonator state is performed using the qubit exactly as for the Fock-state analysis.

In a coherent state the amplitude and phase of the oscillation are well defined, but not the number of photons. A coherent state $|\alpha\rangle$ is a superposition of different Fock states with the probability P_n for an n-photon Fock state following the Poisson distribution

$$P_n(\alpha) = |\langle n|\alpha\rangle|^2 = \alpha^n e^{-\alpha}/n! \qquad (3)$$

that depends on the average photon number α. As a result, the time dependence $P_e(\tau)$ in Fig. 3b is strikingly different from that observed for the Fock states. At low drive amplitude, the response $P_e(\tau)$ is periodic but has low visibility since for $\alpha \ll 1$ all P_n above P_1 are vanishingly small and P_1 itself is small. At higher drive amplitudes, the time traces display a strong initial ringing with fast collapse, followed by a revival—a characteristic feature for a coherent state coupled to a two-level system[26,27]. During the revival, the time dependence is irregular because a coherent state is composed of differ-

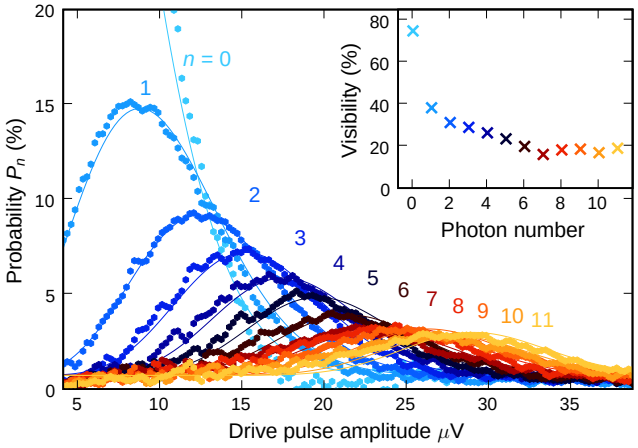

FIG. 4: Population analysis of the coherent state. The dots represent the probabilities P_n for photon number n. They are obtained from the Fourier amplitudes in figure 3d along the dashed vertical lines, translated into photon number probabilities via Eq. (2). Solid lines are the photon number probabilities predicted by the Poisson distribution Eq. 3. They have been scaled by the measurement visibilities shown in the inset. The visibility for $n = 0$ photons is our measurement visibility, the visibilities for higher n are smaller because decoherence lowers the corresponding Fourier amplitudes, increasingly so for higher n.

ent Fock states that oscillate with irrational frequency ratios.

The decomposition of the coherent states into Fock states becomes very clear in the Fourier transform of the time traces, shown in Fig. 3d. The oscillation frequencies coming from different photon numbers appear as sharp vertical lines, indicating the underlying quantum nature of the coherent states. With increasing pulse amplitude, the lines corresponding to higher photon numbers become more pronounced, and at any given pulse amplitude there are several sequential photon numbers with significant occupation probability. In Fig. 3e, the oscillation frequencies corresponding to the maxima of these lines are plotted versus the corresponding photon number. The photon number dependence matches that observed previously in the analysis of the Fock states.

These data also shows good quantitative agreement with the expected Poisson distribution. In Fig. 4 we plot the photon number probabilities P_n obtained from the Fourier amplitude along the dashed vertical lines in Fig. 3d. Their dependence on drive amplitude agrees very well with the Poisson distribution plotted as solid lines. The Poisson distribution has been scaled by a visibility for each photon number n. The visibility for $n = 0$ photons is the measurement visibility. The visibility for higher photon numbers is lower because the Fourier amplitude is reduced by decoherence during the interaction time of 300 ns. We find that shorter interaction times yield much higher visibilities, but at the cost of lower frequency resolution in Fig. 3d and e.

We note that, unlike a pure Fock state, the photon number distribution for a coherent state does not reveal the entire quantum description of the resonator state since a number state analysis cannot by itself distinguish a statistical mixture from a pure coherent state. A full quantum analysis would involve a complete tomographic measurement, yielding, for example, the Wigner function[28]. Given our high fidelity for the Fock state measurements and excellent agreement for the coherent state analysis, we believe that such an experiment should be possible in the near future.

In conclusion, we have created multi-photon Fock states for the first time in a solid-state system. The highest photon number $n = 6$ we have achieved to date is limited only by the coherence times of the qubit and the resonator. In our experiment, the Fock states are created on-demand in a completely deterministic fashion. This opens the possibility of using complex bosonic states in solid-state-based quantum algorithms, which to date have only involved spin-like (fermionic) states.

Acknowledgments

Devices were made at the UCSB and Cornell Nanofabrication Facilities, a part of the NSF-funded National Nanotechnology Infrastructure Network. This work was supported by IARDA under grant W911NF-04-1-0204 and by the NSF under grant CCF-0507227.

* Present address: Ludwig-Maximilians-Universität, Geschwister-Scholl-Platz 1, 80539 München, Germany

[1] Cohen-Tannoudji, C., Diu, B. & Laloe, F. *Quantum Mechanics*, vol. 1 (Wiley & Sons, 2006).
[2] Haroche, S. & Raimond, J.-M. *Exploring the Quantum — Atoms, Cavities and Photons* (Oxford, 2006).
[3] Meekhof, D. M., Monroe, C., King, B. E., Itano, W. M. & Wineland, D. J. Generation of nonclassical motional states of a trapped atom. *Phys. Rev. Lett.* **76**, 1796–1799 (1996).
[4] Cirac, J. I., Blatt, R., Parkins, A. S. & Zoller, P. Preparation of Fock states by observation of quantum jumps in an ion trap. *Phys. Rev. Lett.* **70**, 762–765 (1993).
[5] Varcoe, B. T. H., Brattke, S., Weidinger, M. & Walther, H. Preparing pure photon number states of the radiation field. *Nature* **403**, 743–746 (2000).
[6] Bertet, P. *et al.* Generating and probing a two-photon Fock state with a single atom in a cavity. *Phys. Rev. Lett.* **88**, 143601 (2002).
[7] Waks, E., Dimanti, E. & Yamamoto, Y. Generation of photon number states. *New J. Phys.* **8**, 4 (2006).
[8] Devoret, M. & Martinis, J. M. Implementing qubits with superconducting integrated circuits. *Quantum Inf. Process.* **3**, 163–203 (2004).
[9] Guerlin, C. *et al.* Progressive field-state collapse and quan-

tum non-demolition photon counting. *Nature* **448**, 889–893 (2007).

[10] Wallraff, A. *et al.* Strong coupling of a single photon to a superconducting qubit using circuit quantum electrodynamics. *Nature* **431**, 162–167 (2004).

[11] Johansson, J. *et al.* Vaccum Rabi oscillatoins in a macroscopic superconducnting qubit LC oscillator system. *Phys. Rev. Lett.* **96**, 127006 (2006).

[12] Houck, A. A. *et al.* Generating single microwave photons in a circuit. *Nature* **449**, 328–331 (2007).

[13] Sillanpää, M. A., Park, J. I. & Simmonds, R. W. Coherent quantum state storage and transfer between two phase qubits via a resonant cavity. *Nature* **449**, 438–442 (2007).

[14] Majer, J. *et al.* Coupling superconducting qubits via a cavity bus. *Nature* **449**, 443–447 (2007).

[15] Schuster, D. I. *et al.* Resolving photon number states in a superconducting circuit. *Nature* **445**, 515–518 (2007).

[16] Astafiev, O. *et al.* Single artificial-atom lasing. *Nature* **449**, 588–590 (2007).

[17] Liu, Y.-X., Wei, L. F. & Nori, F. Generation of nonclassical photon states using a superconducting qubit in a microcavity. *Europhys. Lett.* **67**, 941–947 (2004).

[18] Steffen, M. *et al.* State tomography of capacitively shunted phase qubits with high fidelity. *Phys. Rev. Lett.* **97**, 050502 (2006).

[19] Neeley, M. *et al.* Transformed dissipation in superconducting quantum circuits. arXiv:0801.2994 (2008).

[20] Neeley, M. *et al.* Process tomography of quantum memory in a Josephson phase qubit coupled to a two-level state (2008). To be published in Nature Physics.

[21] Devoret, M. H., Esteve, D., Martinis, J. M. & Urbina, C. Effect of an adjustable admittance on the macroscopic energy levels of a current biased Josephson junction. *Phys. Scr.* **T25**, 118–121 (1989).

[22] Devoret, M. H. *et al.* Macroscopic quantum effects in the current-biased Josephson junction. In Kagan, Y. & Leggett, A. J. (eds.) *Quantum Tunnelling in Condensed Media*, chap. 6, 337–338 (Elsevier, 1992).

[23] Jaynes, E. & Cummings, F. Comparison of quantum and semiclassical radiation theories with application to the beam maser. *Proc. IEEE* **51**, 89–109 (1963).

[24] Lucero, E. *et al.* High-fidelity gates in a Josephson qubit. arXiv.org:0802.0903 (2008).

[25] Lu, N. Effects of dissipation on photon statistics and the lifetime of a pure number state. *Phys. Rev. A* **40**, 1707–1708 (1989).

[26] Faist, A., Geneux, E., Meystre, P. & Quattropani, P. Coherent radiation in interaction with two-level system. *Helv. Phys. Acta* **45**, 956 (1972).

[27] Eberly, J. H., Narozhny, N. B. & Sanchez-Mondragon, J. J. Periodic spontaneous collapse and revival in a simple quantum model. *Phys. Rev. Lett.* **44**, 1323–1326 (1980).

[28] Leibfried, D. *et al.* Experimental determination of the motional quantum state of a trapped atom. *Phys. Rev. Lett.* **77**, 4281–4285 (1996).